Received 14 November 2025; Accepted 26 November 2025
https://doi.org/10.48612/letters/2025-4-401-408
https://elibrary.ru/tgjttg

The effect of electrical pulsing on the structure and hardness of highly deformed coarse- and ultrafine-grained aluminum alloy 1570C

O. Sh. Sitdikov, E. V. Avtokratova†, R. R. Zagitov, I. Sh. Valeev, A. Kh. Valeeva,

O. E. Latypova, M. V. Markushev

†avtokratova@imsp.ru

Institute for Metals Superplasticity Problems, Russian Academy of Sciences, Ufa 450001, Russia

Abstract: The study investigates the influence of high-density electropulsing (HDEP) on the microstructure and hardness of non-age-hardenable 1570C aluminum alloy (Al-5.0Mg-0.18Mn-0.20Sc-0.08Zr, wt.%). Interplay between the initial microstructure (coarse-grained (CG) vs. ultrafine-grained (UFG) one), deformation temperature (room temperature rolling (RTR) vs. cryogenic rolling (CR)), and subsequent HDEP was examined. The results demonstrate that cryogenic rolling at −196°C with reduction 80% provides superior hardening (up to 175 HV for UFG + CR) compared to RTR, due to a more non-equilibrium microstructure with higher dislocation density. Subsequent HDEP-induced softening at current densities (K_j) varied from 0.21 to 1.61×10^4 $A^2\cdot s/mm^4$ revealed a strong dependence of the microstructure and hardness of alloy on its initial state. The alloy in CG + RTR condition exhibited the highest thermal stability and gradual softening via recovery. In contrast, the alloy in UFG + CR state with the highest stored energy softened most rapidly, initiating recrystallization at the lowest values of energy threshold. A key finding is the formation of a kinetically stable, partially recrystallized bimodal structure in the alloy in UFG + CR state after HDEP, resulting from the competition between a high driving force for recrystallization and the Zener pinning effect of nanoscale $Al_3(Sc,Zr)$ dispersoids. After high-energy pulsing, the hardness for all states converged to a level near the initial homogenized condition (≈100 HV), signifying a fundamental shift from deformation-based strengthening back to solid solution and dispersion hardening.

Keywords: aluminum alloy, nanoscale dispersoids, cold rolling, high-density electric pulsing, microstructure, hardness

Acknowledgements: *The work was carried out both with the support of the Russian Science Foundation under grant №23-19-00702 (https://rscf.ru/en/project/23-19-00702/) (for cryogenic rolling) and under the state assignment of IMSP RAS (for room-temperature rolling). Experimental studies were carried out on the facilities of shared services center of IMSP RAS.*

1. Introduction

The pursuit of enhanced mechanical properties in aluminum alloys has long driven the development of thermomechanical processing routes. For non-age-hardenable alloys, such as those from the 5XXX series, strengthening is primarily achieved through strain hardening [1, 2]. However, subsequent annealing to improve the structure often leads to excessive recrystallization and grain growth, which can compromise the strength [3]. To overcome these limitations, advanced processing techniques combining severe plastic deformation with fast heat treatment have gained significant attention.

Among these, high-density electropulsing (HDEP) has emerged as a promising method for microstructural control. The application of short, high-energy current pulses can activate recovery and recrystallization processes with exceptional speed, often leading to the formation of finer grains. Studies on cryogenically deformed pure FCC metals have demonstrated that post-deformation HDEP can produce homogeneous ultrafine grained (UFG) structures or nanoscale dislocation arrays [4, 5].

However, the response of complex aluminum alloys containing transition elements such as Sc and Zr to such combined processing remains less explored. The presence of nanoscale $Al_3(Sc,Zr)$ dispersoids strongly inhibits dislocation rearrangement and retards recrystallization [6], making the microstructural evolution during HDEP markedly different from that in pure metals [7]. The 1570C alloy (Al-Mg-Mn-Sc-Zr), with its combination of solid solution and dispersion hardening, represents an ideal model system for investigating these interactions.

This study examines the influence of HDEP on the microstructure and hardness of work-hardened 1570C alloy in two distinct initial conditions, primarily differing in grain size. It systematically extends our previous investigation on the response of coarse-grained (CG) 1570C alloy to electropulsing [7] by incorporating a severely deformed

UFG condition. This comparative approach provides a comprehensive view of the microstructure-HDEP property relationships across a wide spectrum of initial defect states, from a work-hardened coarse-grained structure to an extremely defective nano-substructured UFG material. The aim of the work is to elucidate how initial microstructure and deformation temperature affect the structural stability and softening behavior of the alloy under electropulsing, with a particular focus on the competition between recovery and recrystallization in these fundamentally different starting conditions.

2. Material and experimental methods

2.1. Material and pre-processing

The investigation was conducted on a commercial 1570C aluminum alloy with the following chemical composition (in wt.%): Al-5.0Mg-0.18Mn-0.20Sc-0.08Zr-0.01Fe-0.01Si. To elucidate the influence of the initial microstructure, the study focused on two distinct material states. The first was a CG condition of a homogenized ingot, and the second was an UFG alloy, processed by multi-directional forging of the first one.

2.2. Rolling

Plate-shaped specimens were machined from the alloy in both the CG and UFG states and subjected to severe plastic deformation via rolling to a total true strain of 80%. To evaluate the influence of deformation temperature, the rolling was performed under two distinct regimes: at room temperature (RTR) of 25°C and at a cryogenic temperature (CR) of −196°C in liquid nitrogen. The CR process was conducted under isothermal conditions, ensured by cooling both the specimens and the work rolls in a liquid nitrogen bath. This approach effectively suppresses dynamic recovery, thereby promoting a higher accumulation of lattice defects and the formation of a more non-equilibrium microstructure compared to room-temperature deformation.

2.3. HDEP Treatment

The work-hardened samples were subsequently subjected to HDEP. A single decaying sinusoid current pulse with a duration of 100 μs was applied using a specialized generator. The treatment intensity was controlled by the integral current density parameter, K_j, which was varied systematically from 0.21 to 1.61×10^4 $A^2\cdot s/mm^4$. Specimens with the "dog-bone" geometry were employed. Following electropulsing, all samples were stored at −18°C to preserve the induced microstructural states prior to further analysis.

2.4. Microstructural characterization and hardness testing

The evolution of microstructure was characterized using a combination of electron microscopy techniques. The general microstructure and crystallographic features were analyzed by Scanning Electron Microscopy (SEM) equipped with an Electron Backscatter Diffraction (EBSD) system. The EBSD maps were acquired on the transverse plane, perpendicular to the rolling direction (RD), and processed to identify boundaries based on their misorientation angles: low-angle boundaries (LABs, $2°\leq\Theta<5°$, grey color), medium-angle boundaries ($5°\leq\Theta<15°$, red color), and high-angle boundaries (HABs, $\Theta\geq15°$, black color). For a detailed analysis of the dislocation substructure, transmission electron microscopy (TEM) was employed. Specimens for SEM/EBSD and thin foils for TEM examinations were prepared by electropolishing in a 30% HNO_3 + 70% CH_3OH solution at −28°C.

The mechanical behavior of the alloy was evaluated through Vickers microhardness (HV) measurements. The tests were performed on the rolling plane at room temperature with a load of 0.5 N. Each reported hardness value represents the average of at least ten individual indentations to ensure statistical reliability.

3. Results and discussions

3.1. Initial material states before HDEP

To systematically investigate the influence of the initial microstructure on the response to HDEP, four distinct work-hardened states of the 1570C alloy were prepared. These states were characterized by different initial grain structures (CG and UFG) and subsequent deformation paths (RTR and CR), which resulted in a wide range of defect densities and microstructural configurations. The key parameters of these states are summarized in Table 1.

3.1.1. CG ingot states

The baseline material was a homogenized CG ingot featuring an equiaxed microstructure with an average grain size of 25 μm and a low initial dislocation density of ~10^{12} m^{-2} (Fig. 1a, d, g, j) [8, 9]. TEM analysis revealed the presence of evenly distributed nanoscale $Al_3(Sc,Zr)$ dispersoids with an average diameter of 10–15 nm and a spatial density of approximately 1×10^4 μm^{-3} (Fig. 1j) [9]. Their coherency with the aluminum matrix was confirmed by the distinct "coffee-bean" strain field contrast observed in the bright-field TEM images [11]. This initial alloy state, with a microhardness of ≈105 HV, served as the precursor for the following two work-hardened conditions:

Table 1. Microstructural parameters and hardness of the 1570C alloy in the work-hardened states.

Material Condition	Dislocation Density (m^{-2})	Coherent Domain Size (nm)	Microhardness (HV)
CG (Ingot + RTR) [7]	$\approx3.5\times10^{13}$	≈50	140 + 5
CG (Ingot + CR) [8, 7]	$\approx5.9\times10^{14}$	≈24	155 + 5
UFG (Forging + RTR) [9]	$\approx3.5\times10^{14}$	≈59	160 + 6
UFG (Forging + CR) [10]	$\approx9.0\times10^{14}$	≈15	176 + 5

(i) CG ingot after room-temperature rolling (CG + RTR). Cold rolling at 25°C to a total strain of ε = 80% resulted in significant work hardening, increasing the microhardness to ≈140 HV. The microstructure evolved into a well-defined cell- and deformation band structure (Fig. 1b, e, h, k). Within the elongated original grains, microshear bands with misorientations up to 5 – 10° were formed, which is typical for cold rolling of aluminum alloys with high stacking fault energy [12].

(ii) CG ingot after cryogenic rolling (CG + CR). Rolling at −196°C led to even greater strengthening, with the hardness reaching ≈155 HV. The structural response to cryogenic deformation was notably different (Fig. 1c, f, i, l). Instead of well-defined microshear bands, a more diffuse, weakly misoriented cell/deformation structure was formed, characterized by the one-order higher dislocation density and by the twice smaller coherent domain size compared to the room-temperature rolling condition (see Table 1). This indicates a more non-equilibrium structural state, which can be attributed to the suppression of dynamic recovery and a more homogeneous activation of multiple slip systems at cryogenic temperatures [13,14].

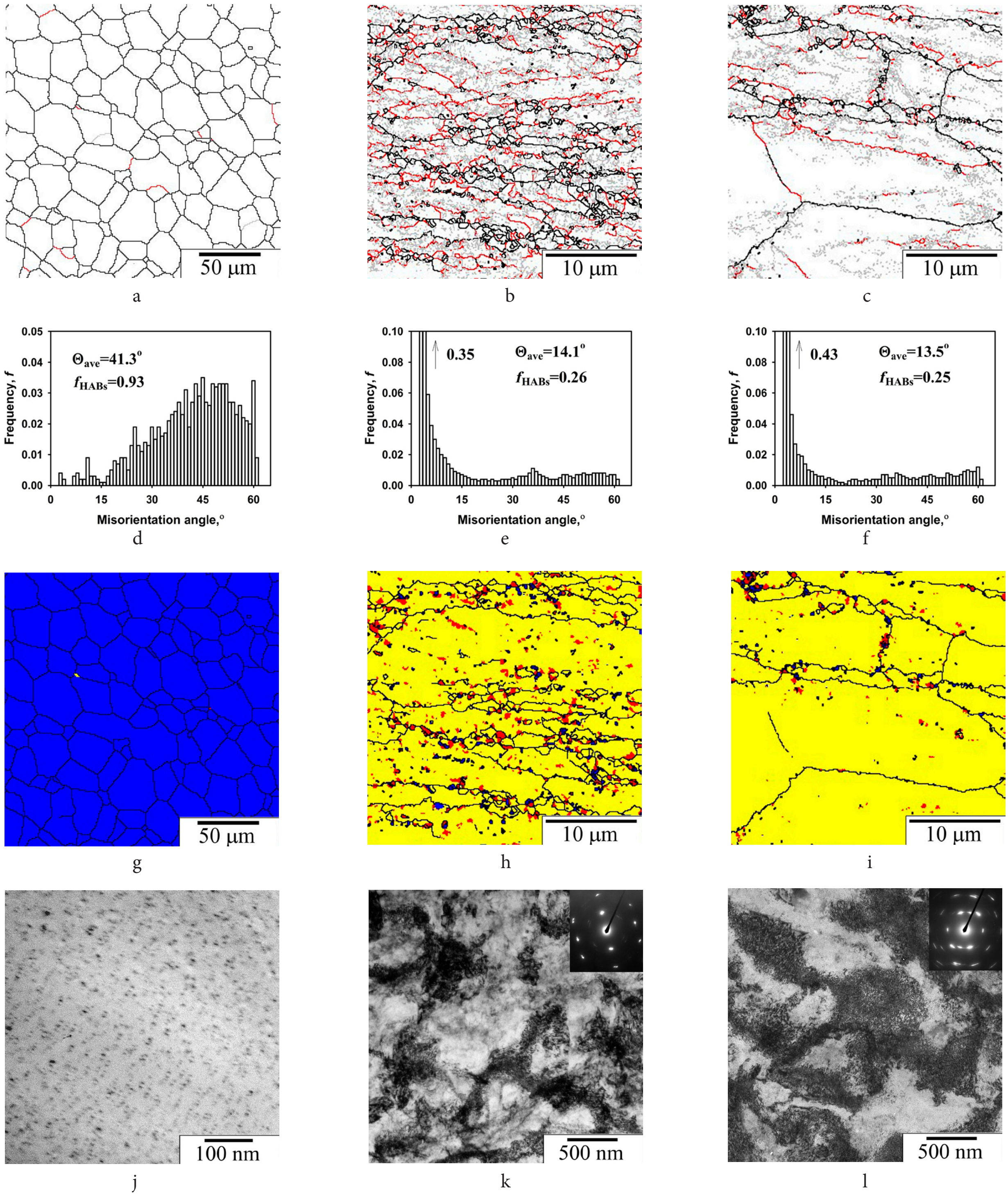

Fig. 1. (Color online) EBSD (a – i) and TEM (j – l) images of the microstructure of the 1570C alloy in the CG state (a, d, g, j) with subsequent RTR (b, e, h, k) or CR (c, f, i, l). Hereafter on the EBSD recrystallization maps (Fig. 2 g – i, Fig. 3 g – i, and Fig. 4i – l), the red/yellow/blue colors highlight the deformed/substructured/recrystallized regions, respectively.

3.1.2. UFG forged billet states

The initial UFG structure was produced by subjecting the homogenized ingot to multidirectional isothermal forging at 325°C to a cumulative strain of ≈12. This process resulted in a nearly homogeneous UFG structure with an average grain size of about 2.0 μm (Fig. 2a, d, g, j) [9,10]. The microhardness of the alloy in this forged state (≈105 HV) was comparable to the one of initial homogenized ingot.

This could be explained by a dualism of strengthening and softening mechanisms: the Hall-Petch strengthening from significant grain refinement was compensated by the coarsening of coherent $Al_3(Sc,Zr)$ dispersoids and a reduction in their spatial density during high-temperature deformation [9]:

(i) UFG after room-temperature rolling (UFG + RTR). Subsequent rolling of the UFG billet at 25°C to ε = 80% effectively transformed the relatively equilibrium forged structure into a severely work-hardened structural state (Fig. 2b, e, h, k), raising the hardness to ≈160 HV. The microstructure was characterized by an elongated grain morphology with a high density of low-angle boundaries [9].

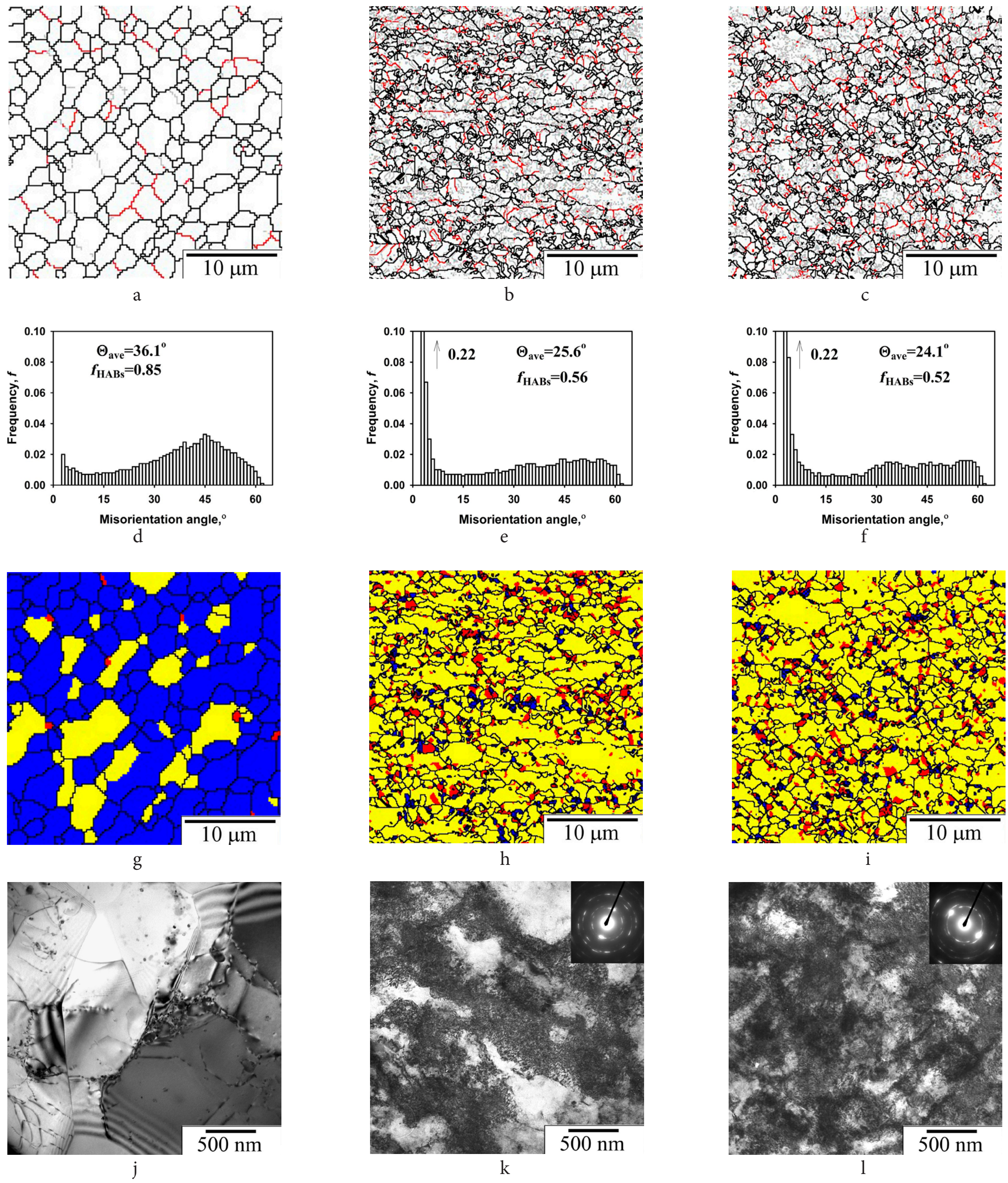

Fig. 2. (Color online) EBSD (a – i) and TEM (j – l) images of the microstructure of the 1570C alloy in the UFG state (a, d, g, j) with subsequent RTR (b, e, h, k) or CR (c, f, i, l).

(ii) UFG after cryogenic rolling (UFG + CR). This combination of processing routes yielded the most extreme work-hardened state. Cryogenic rolling of the UFG billet to a reduction of 70 – 90% resulted in the highest hardness of ≈176 HV. The structure was characterized by an exceptionally high dislocation density approaching approximately 10^{15} m^{-2} and the smallest coherent domain size of ≈15 nm (Table 1) [10]. The UFG structure was transformed into a highly non-equilibrium, nano-substructured state where intense grain subdivision occurred (Fig. 2 c, l), and dislocation boundaries were effectively pinned by the nanoscale dispersoids.

In summary, these values highlight the significant difference in how the alloy structure responds to different rolling temperatures. Cryogenic rolling results in a much higher dislocation density and a finer coherent domain size, explaining the greater hardness increase compared to room-temperature rolling. The four initial states provided a spectrum of microstructural conditions, from a work-hardened coarse-grained structure (CG + RTR) to an extremely defect nano-substructured UFG material (UFG + CR), thereby creating a solid basis for studying their respective responses to subsequent HDEP.

3.2. Effect of HDEP on structure and hardness

3.2.1. Hardness evolution and softening behavior

The alloy in the work-hardened states described in Sections 3.1.1 and 3.1.2 was subjected to HDEP with varying integral current density (K_j). A general trend of decreasing hardness with increasing K_j was observed for all four states, as summarized in Fig. 3. However, the extent of softening, the energy thresholds for microstructural changes, and the underlying mechanisms were strongly dependent on the initial microstructure and deformation temperature.

The alloy in the CG+RTR state demonstrated the highest stability under HDEP. Its hardness decreased monotonically and gradually up to the highest applied K_j value of 1.23×10^4 A^2·s/mm^4, where the hardness approached ≈120 HV. This indicates a remarkable resistance to HDEP-induced annealing, primarily governed by static recovery over a wide energy range.

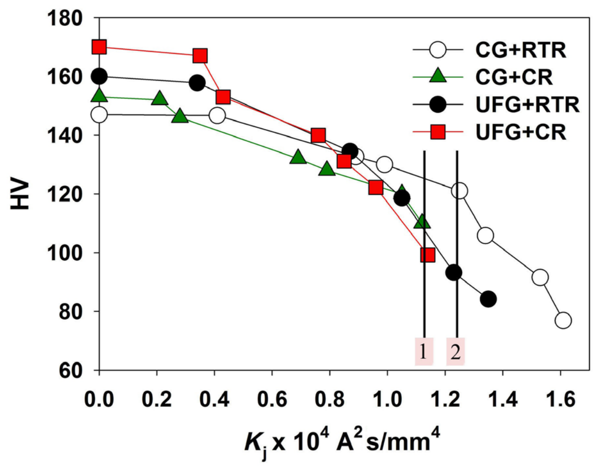

Fig. 3. (Color online) Microhardness of 1570C alloy in the CG and UFG states subjected to rolling at room and cryogenic temperatures and subsequent HDEP. The lines 1 and 2 correspond to the states whose microstructures are represented in the paper.

In contrast, the UFG + CR state, which had the highest initial defect density, softened most rapidly and intensely. A sharp drop in hardness was observed to start at a comparatively lower K_j threshold of 0.96×10^4 A^2·s/mm^4, where the hardness reached the same value of ≈120 HV. This signifies lower stability and a high driving force for recrystallization due to the immense stored energy. The softening behavior of the alloy in the CG + CR and UFG + RTR states was intermediate. The CG + CR state began significant softening at lower energies compared to its room-temperature rolled counterpart, while the UFG + RTR state showed a steeper decline in hardness than the CG + RTR state, underscoring the influence of both initial grain size and deformation temperature.

Analysis of the hardness curves allowed for the identification of three distinct intervals of K_j, corresponding to the dominance of different restoration processes:

(i) Interval I (low K_j). At energies up to 0.43×10^4 A^2·s/mm^4, hardness remained relatively stable for most states, with minor softening attributed to the initial stages of recovery.

(ii) Interval II (intermediate K_j). In the range of approximately 0.43 to 1.05×10^4 A^2·s/mm^4, a near-linear decrease in hardness was observed, dominated by widespread static recovery. For the UFG + CR state, this interval also saw the onset of recrystallization.

(iii) Interval III (high K_j). At energies above $0.96 – 1.05 \times 10^4$ A^2·s/mm^4, a sharp drop in hardness occurred, signaling the activation of large-scale static recrystallization. As stated above, this was most pronounced for the cryogenically rolled states (CG + CR and UFG + CR), while the CG + RTR state required energies above 1.25×10^4 A^2·s/mm^4 to enter this stage.

Ultimately, HDEP led to significant softening of the alloy in all states, with the hardness converging to a value of approximately 90 ± 15 HV, which is close to or even less than the hardness in the annealed alloy condition.

3.2.2. Microstructural response to HDEP

The microstructural evolution observed via EBSD and TEM directly correlated with the hardness intervals described in Section 3.2.1, revealing distinct restoration mechanisms.

(i) At low K_j values, the primary process was static recovery, characterized by the rearrangement and annihilation of dislocations, leading to sharper and cleaner subgrain boundaries without significant changes in their misorientation angles, as consistent with our earlier detailed analysis [7]. This process was predominant in the CG + RTR state across the widest energy range, up to $K_j \approx 0.41 \times 10^4$ A^2·s/mm^4, which explains its high thermal stability and gradual softening. In the UFG and/or cryogenically rolled states, which possessed a higher density of non-equilibrium boundaries, recovery also initiated at these low energies but was accompanied by a more noticeable reduction in dislocation density within the cells/subgrains.

(ii) At intermediate K_j values, the onset of recrystallization was observed, particularly in the states with high stored energy. For instance, in the cryogenically rolled CG + CR alloy, new strain-free grains nucleated primarily in regions of highest defect density, such as microshear bands and initial grain boundaries — a phenomenon thoroughly characterized in our companion paper [7] (Fig. 4 a, e, i, m). A key finding in this interval was the alloy behavior in the UFG + CR state. Even in this interval, it was characterized by a developed partially recrystallized bimodal (sub)grain structure (Fig. 4 b, f, j, n). This structure consisted of fine, recovered subgrains and new, strain-free recrystallized grains.

(iii) At high K_j values, recrystallization and grain growth became widespread. In the UFG + RTR and UFG + CR states, this resulted in the formation of more numerous, albeit (ultra)fine, recrystallized grains (as shown for the UFG + RTR state in Fig. 4 d, h, l, p). In stark contrast, the CG+RTR state still required the highest energy inputs to initiate this stage (see Fig. 4 c, g, k, o), consistent with its highest stability.

3.3. Discussion on structural stability under HDEP

The differential response of the four work-hardened states to HDEP is primarily attributed to the magnitude of the stored energy and the specific nature of the defect structure introduced during prior straining.

The alloy in UFG + CR state, possessing the highest dislocation density (almost 10^{15} m^{-2}) and a high fraction of non-equilibrium boundaries, had an extremely high driving force for recrystallization. This explains its rapid and intense softening, which initiated at the lowest K_j threshold values. A key finding was the formation of a bimodal, partially recrystallized structure, which persisted even at the highest K_j values investigated (Fig. 4 b, f, j, n), despite a significant hardness drop. This behavior stands in stark contrast to

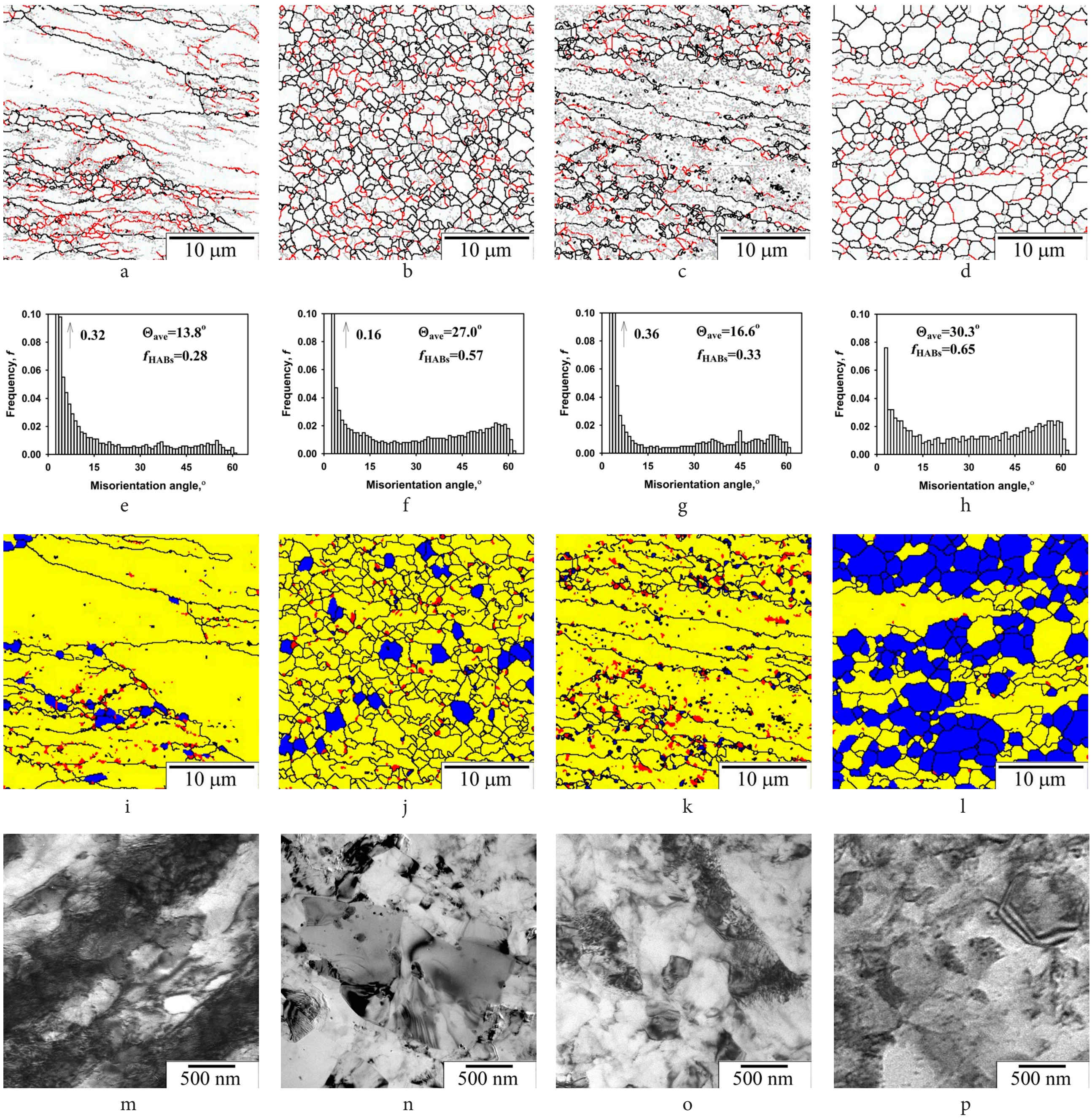

Fig. 4. (Color online) EBSD (a – l) and TEM (m – p) images of the microstructure of the 1570C alloy after: CR and HDEP with K_j=1.1×10^4 A^2·s/mm^4 (line 1 in the Fig. 3) in the CG state (CG + CR) (a, e, i, m) and in the UFG state (UFG + CR) (b, f, j, n); RTR and HDEP with K_j=1.2×10^4 A^2·s/mm^4 (line 2 in the Fig. 3) in the CG state (CG + RTR) (c, g, k, o) and in the UFG state (UFG + RTR) (d, h, l, p).

pure FCC metals like Ni, Cu, and Al, where the absence of such strong pinning particles allows cryogenic rolling and subsequent HDEP to produce a fully recrystallized microstructure [15,16]. The persistence of the partially recrystallized state in the 1570C alloy underscores the critical role of nanoscale dispersoids in controlling the final microstructural outcome during electropulsing.

Conversely, the CG+RTR state, with a lower initial defect density and a more stable, well-defined dislocation/cell structure, relaxed its stored energy gradually through extended recovery [17,18]. As established in [7], the slower rearrangement and annihilation of lattice dislocations within these more equilibrium boundaries resulted in greater resistance to recrystallization, requiring the highest energy inputs to initiate noticeable grain nucleation and growth.

The softening kinetics and microstructural evolution of the two other moderately-to-highly strained alloys, CG + CR and UFG + RTR, demonstrated an intermediate character, as clearly evidenced by their positions on the hardness curves (Fig. 3) and their transitional microstructures (Fig. 4). The CG + CR alloy, with its high dislocation density but coarser initial grain size, softened faster than the CG + RTR one but more slowly than UFG + CR. Similarly, the alloy in UFG + RTR state, with its refined initial grain size but lower dislocation density compared to UFG + CR, exhibited a stability higher than that of the cryogenically rolled states but lower than that of the CG + RTR alloy.

Furthermore, the convergence of hardness for all alloy states to a level of ≈80 – 100 HV after high-energy HDEP — comparable to or even below the hardness in the initial homogenized condition and aligning with the final softening stage documented for the CG states in [7] — signifies a fundamental shift in the dominant strengthening mechanisms throughout the entire thermomechanical treatment process. In the work-hardened states, strength was governed by a potent combination of grain boundary strengthening (Hall-Petch), dislocation strengthening, and dispersion hardening [18,19]. The post-HDEP recrystallization process, however, leads to the simultaneous coarsening of the grain structure and annihilation of dislocations [15,16]. Consequently, the contributions from Hall-Petch and dislocation strengthening are effectively eliminated. The resulting mechanical properties are thus primarily determined by solid solution and dispersion strengthening — the very same mechanisms that dominated in the initial annealed state [19, 20]. Some variations in final hardness can be attributed to differences in the final grain size and the possible relaxation (partial coherency loss) of the dispersoid-matrix interfaces after rapid electropulsing.

The above interpretation resolves the paradox of a sharp hardness drop co-occurring with only a partially recrystallized, bimodal structure in the UFG + CR state. The explanation lies in the selective and kinetically limited nature of recrystallization in this alloy. The process initiates in the regions of highest defect density, where the driving force is maximal. The rapid formation of these strain-free grains consumes the areas that contributed most significantly to dislocation strengthening, leading to an immediate and pronounced drop in hardness [18]. Simultaneously, the Zener pinning from nanoscale $Al_3(Sc,Zr)$ dispersoids kinetically hinders complete boundary migration [11,17,18]. This competition results in a stable, bimodal microstructure of recrystallized grains embedded in a recovered, dislocation-rich matrix (Fig. 4), where the hardness reflects the loss of the strongest strengthening component, while the pinning dictates the incomplete transformation.

In summary, the results demonstrate that the combination of the initial grain structure and the deformation temperature dictates the pathway and kinetics of structural relaxation under HDEP. The stored energy defines the driving force for restoration processes (recovery and recrystallization), while the morphology of the defect structure as well as the pinning by dispersoids control the kinetics and final microstructural outcome. This understanding provides a baseline for tailoring microstructural evolution in advanced aluminum alloys through a combination of thermomechanical processing, including cryogenic rolling and HDEP.

4. Conclusions

The effect of high-density electropulsing (HDEP) on the work-hardened 1570C aluminum alloy leads to the following main conclusions:

1. Cryogenic rolling is a more effective strengthening method than room-temperature rolling, achieving a peak hardness of 175 HV. This superiority is attributed to the formation of a highly non-equilibrium microstructure with an elevated dislocation density, resulting from the suppression of dynamic recovery.
2. The structural stability under HDEP is dictated by the initial state. The coarse-grained, room-temperature rolled (CG + RTR) alloy exhibits the highest stability, softening via recovery, while the ultrafine-grained, cryogenically rolled (UFG + CR) alloy with the highest stored energy is the least stable, undergoing rapid recrystallization. The CG + CR and UFG + RTR states demonstrate intermediate softening kinetics.
3. A key outcome is the formation of a stable, bimodal partially recrystallized microstructure in the UFG + CR state after HDEP. This structure results from the competition between a high driving force for recrystallization and the potent Zener pinning effect of nanoscale $Al_3(Sc,Zr)$ dispersoids.
4. High-K_j HDEP causes the hardness in all alloy states to converge to ≈100 HV, near the initial homogenized condition. This signifies a fundamental change in the dominant strengthening mechanisms, from deformation-based (grain boundaries and dislocations) to solid solution and dispersion hardening.

References

1. E.L. Huskins, B. Cao, K.T. Ramesh, Strengthening mechanisms in an Al-Mg alloy, Mater. Sci. Eng. A 527 (2010) 1292 – 1298.
2. B. Yang, Yu Wang, M. Gao, Ch. Wang, R. Guan, Microstructural evolution and strengthening mechanism of Al-Mg alloys with fine grains processed by accumulative continuous extrusion forming, J. Mater. Sci. Technol. 128 (2022) 195 – 204.

3. T. Tański, P. Snopiński, K. Prusik, M. Sroka, The effects of room temperature ECAP and subsequent aging on the structure and properties of the Al-3%Mg aluminium alloy, Mater. Charact. 133 (2017) 185–195.
4. M. Markushev, I. Valeev, A. Valeeva, R. Ilyasov, E. Avtokratova, S. Krymskiy, O. Sitdikov, Effect of electric pulsing on the structure, texture and hardness of cryorolled fine-grain copper, Facta Universitatis, Ser: Mech. Eng. (2022).
5. M.V. Markushev, E.V. Avtokratova, A.Kh. Valeeva, I.Sh. Valeev, R.R. Ilyasov, S.V. Krymsky, O.Sh. Sitdikov, Combination of cryogenic deformation and electropulse processing as a way to produce ultrafine-grain metals, Frontier Mater. Technol. 4 (2023) 53–62.
6. P.J. Apps, M. Berta, P.B. Prangnell, The Effect of Dispersoids on the Grain Refinement Mechanisms during Deformation of Aluminium Alloys to Ultrahigh Strains, Acta Materialia 53 (2005) 499–511.
7. O.S. Sitdikov, E.V. Avtokratova, R.R. Zagitov, S.V. Krymskiy, I.S. Valeev, A.K. Valeeva, O.E. Latypova, M.V. Markushev, Structure and hardness of 1570C aluminum alloy after room- and cryogenic temperature rolling and electrical pulsing, Lett. Mater. 14 (4) (2024) 439–445.
8. O.Sh. Sitdikov, E.V. Avtokratova, R.R. Zagitov, S.V. Krymskiy, O.E. Latypova, M.V. Markushev. Structure and mechanical properties of AL-5%Mg-Sc-Zr alloy after ceryogenic deformation. Russ. Phys. J. 67 (10) (2024) 1501–1508.
9. E. Avtokratova, O. Sitdikov, M. Markushev, M. Linderov, D. Merson, A. Vinogradov, The processing route towards outstanding performance of the severely deformed Al-Mg-Mn-Sc-Zr alloy. Mater. Sci. Eng. A 806 (2021) 140818.
10. O.Sh. Sitdikov, E.V. Avtokratova, R.R. Zagitov, O.E. Latypova, S.V. Krymskiy, M.V. Markushev, Microstructure and mechanical properties of multidirectionally forged Al alloy 1570C subjected to cryogenic rolling. Int. J. Lightweight Mater. Manufact. (2025) in press.
11. T.-S. Liu, B.-X. Dong, H.-Y. Yang, F. Qiu, S.-L. Shu, Q.-C. Jiang, Review on role of intermetallic and ceramic particles in recrystallization driving force and microstructure of wrought Al alloys, J. Mater. Res. Technol. 27 (2023) 3374–3395.
12. P.J. Hurley, F.J. Humphreys, The application of EBSD to the study of substructural development in a cold rolled single-phase aluminium alloy, Acta Mater. 51 (2003) 1087–1102.
13. G.E. Totten, D.S. MacKenzie, Handbook of Aluminum, Volume 2: Alloy Production and Materials Manufacturing, New York, CRC Press (2003) 736 p.
14. P.A. Khaimovich, Cryodeformation of metals under isotropic compression (Review), Low Temp. Phys. 44 (2018) 349–370.
15. M.V. Markushev, I.Sh. Valeev, E.V. Avtokratova, R.R. Ilyasov, A.Kh. Valeeva, S.V. Krimsky, O.Sh. Sitdikov, Effect of high-dense electropulsing with different energies on the structure and strength of nickel cryorolled to different strains, Lett. Mater. 13 (2) (2023) 126–131.
16. M.V. Markushev, R.R. Ilyasov, S.V. Krymskiy, I.S. Valeev, O.S. Sitdikov, Structure and strength of fine-grain copper after cryorolling and single electro-pulsing of different capacity, Lett. Mater. 11 (4) (2021) 491–496.
17. F.J. Humphreys, M. Hatherly. Recrystallization and Related Annealing Phenomena, 2nd ed. Elsevier, Amsterdam (2004) 658 p.
18. K. Huang, R.E. Logé, A review of dynamic recrystallization phenomena in metallic materials, Mater. Des. 111 (2016) 548–574.
19. A. Kostryzhev, Strengthening Mechanisms in Metallic Materials, Metals. 11 (7) (2021) 1134.
20. E. Avtokratova, O. Sitdikov, O. Mukhametdinova, M. Markushev, S.V. S. N. Murty, M.J. N. V. Prasad, B.P. Kashyap, Microstructural evolution in AleMgeSceZr alloy during severe plastic deformation and annealing, J. All. Comp. 673 (2016) 182–194.